6

Original Study

Heide Wrobel Nørgaard*

Portable XRF on Prehistoric Bronze Artefacts: Limitations and Use for the Detection of Bronze Age Metal Workshops

https://doi.org/10.1515/opar-2017-0006 Received September 29, 2016; accepted May 23, 2017

Abstract: Two different scientific analyses—one destructive and one non-destructive—were conducted on two separate groups of bronze ornaments dating from 1500–1100 BC to investigate, amongst other traits, the metal composition of their copper-tin alloys. One group of artefacts was sampled, and polished thin sections were analysed using a scanning electron microscope (SEM). Results from the corrosion crust of copper-tin alloys, and the change measured within the elemental composition from the bulk metal to the surface, greatly influenced the interpretation of the second data set, which was measured using a handheld X-ray fluorescence (XRF) device. The surface of corroded bronze ornaments consists mostly of copper carbonates, oxides, and chlorides. Chemical processes, such as decuprification, change the element composition in such a manner that the original alloy cannot be traced with a non-destructive method. This paper compares the results of both investigations in order to define the possibilities and limits of non-destructive XRF analyses of corroded bronze artefacts.

Keywords: portable XRF-analysis, corroded bronze ornaments, determination of workshops, Nordic Bronze Age

1 Introduction

Defining metal workshops using scientific methods—for instance, through analysis of trace elements or isotopic signatures—is a common matter of interest in archaeometallurgical studies. However, since the middle of the nineteenth century, the impact of chemical analysis in provenancing archaeological objects was discussed with a focus on the definition of workshops (for a detailed research history, see Pernicka 2014, Stos-Gale & Gale 2009).

Behind such an approach is the assumption that the metalworker was well aware of the properties of the metal in use and intentionally chose that best suited to the object's purpose. The colour, smell, and weight of the metal, as well as its reaction during smelting, would have given the craftsperson all the information needed to successfully produce the desired copper alloy. This can also be inferred for bronze and, as such, the already alloyed tin-bronze would have been specifically chosen by the craftsperson to meet further need. To support such a statement, however, a detailed trace element analysis of artefacts produced within one defined workshop is necessary.

Article note: This article is a part of Topical Issue on Portable XRF in Archaeology and Museum Studies

^{*}Corresponding author: Heide Wrobel Nørgaard, Aarhus University, Institute for Culture and Society, DK-8270 Højbjerg, E-mail: farkhw@cas.au.dk

Within a FP7-financed project, several metal workshops were detected from the early and middle Nordic Bronze Age—namely in southern Scandinavia, Denmark, and North Germany (see Nørgaard 2014a, 2014b, 2015b, 2015c).

Based on traces visible on the material culture, such as tool marks, residues of the crafting (technical traces), and relics of the craftsperson's habitus, eleven NBA II (1500–1350 BC) workshops were defined in Denmark. Five further workshops were detected in Lower Saxony, including four NBA III (1350–1100 BC) workshops in Mecklenburg, with evidence pointing towards a continuation of the majority of the NBA II workshops. This project raised the possibility of testing for intentional alloying, and thus identifying a specific craftsman through a signature alloy. The material from Mecklenburg (NBA III) offered a potentially insightful case study, as the technical defined workshops, while located within a narrow region, clearly could be separated due to their characteristics (Nørgaard 2015a). Furthermore, the availability of the material promised a robust data set. However, given the tendency within modern archaeology to emphasise the protection and preservation of artefacts, solely a non-destructive analytical approach was allowed.

Non-destructive methods are becoming increasingly important within modern archaeological research. These methods include analysis by handheld XRF spectrometer (Anker 1982, Helfert & Böhme 2010, Wolff 2009). Advancements in the scientific analysis of prehistoric objects, without the risk of damage, promise researchers access to previously hidden information. Furthermore, the increasing availability of portable XRF devices, as well as their moderate cost when compared to laboratory-based technologies, more frequently allows the incorporation of chemical examinations in material culture studies. However, such analyses have their limits and not all questions can be answered in this manner.

One major difficulty in the non-destructive analysis of bronze artefacts in museum collections or in the field is the fact that the majority of these objects are corroded. Several studies have concentrated on the analysis of corrosive structures on copper alloy objects (e.g. Bernard & Joiret 2009, Chase 1994, Constantinides, Adrianes, & Adams 2002, Mircea, Sandu, Vasilache, & Sandu 2012, Oudbashi, Emami, Ahmadi, & Davami 2013, Robbiola, Blengino, & Fiaud 1998, Wadsak et al. 2000), while only a small number have discussed the analysis of corroded artefacts using handheld XRF devices (Fernandes, van Os, & Huisman 2013, Šatović, Desnica, & Fazinić 2013). Unfortunately, these studies are typically published within the domain of conservation studies and seldom find their way to archaeologists. Nonetheless, within archaeological literature, the difficulties involved in using superficial analytical methods to determine the composition of copper alloys in ancient artefacts have been mentioned and researchers have also noted the fact that those values measured superficially using these methods give little insight about the actual alloy (e.g. Härke 1978, Lutz & Pernicka 1996, Otto 1973, Pernicka 2010). However, this topic is rarely discussed at any length (exceptions i.e. Pernicka 2010, 720-724), perhaps permitting archaeology's continued assumption that an analysis of the surface of corroded bronze artefacts will allow one to determine the composition of the underlying alloy. The following case study will demonstrate not only the degree of the advancement of corrosion on a select set of Northern European bronze artefacts, but also the value to be gained by the nondestructive analysis of such objects. As such, this paper contributes to a wider debate regarding the limits of non-destructive analysis using portable XRF technology. It will discuss the kinds of questions that could be answered using handheld XRF and whether a surface analysis of artefacts will allow the determination of workshops via the trace element composition.

2 Material and Method

To illustrate the limits of non-destructive methods such as XRF, outlined above, this study describes two differently-executed analyses of corroded bronze ornaments originating within and dated to the Nordic Bronze Age (1500–1100 BC). The material considered here consists of belt plates and neck collars from NBA II sites (1500–1300 BC) in Lower Saxony (Nørgaard 2015b) and from NBA III sites (1300–1100 BC) in Mecklenburg, Germany (Nørgaard 2015a). All artefacts examined for this study are made from bronze, a copper-tin alloy, and form part of existing museum collections or stores. The majority of objects within the sample were acquired at the beginning of the twentieth century; thus, many of the bronzes are coated with

a heavy corrosion layer, and sometimes even with a layer of varnish or paint. They represent the normal spectra of bronze artefacts a researcher will find while investigating the Bronze Age in northern Europe.

As this paper focuses on the possibilities and limits of non-destructive XRF-analysis in the study of bronze artefacts, rather than the craft of metalworking itself¹, the differences within the analytical methods of both object groups and their potential regarding the leading question is the main objective. To this end, this study considers primarily the corrosion of the examined artefacts and its effect on the chosen analytical method.

An earlier study details the metallographic analysis of the NBA II ornaments from Lower Saxony considered here (Nørgaard 2015b); the results of that investigation made it possible to reconstruct the detailed operational sequence of the crafting process (Nørgaard 2014a, 680ff.). During this earlier analysis at the German Mining Museum in Bochum, it was possible to perform a more extensive investigation of the specimen, due to a fully exposed cross-section. With the objective of defining the corrosion layers of the bronze artefacts, as well as the change in the alloy composition towards the objects' surface, the samples were examined under a scanning electron microscope (SEM). The specimen samples were placed within the large sample chamber (no restricting airlock) of the field emission scanning electron microscope (SUPRA 40 VP from Zeiss), located in the museum's material science laboratory. The SEM is equipped with an energy-dispersive x-ray spectrometer (Noran System 7, Thermo) with a silicon drift detector (SDD). In order to execute further metallographic investigations under the light microscope, the sand-polished specimen samples were placed within a Bakelite ring and labeled on the back (Nørgaard 2015b). The results from the scanning process allowed the author to determine the alloy compositions of the artefact and the changes within the composition towards the corrosion and within the corrosion layer. To offer a detailed characterisation of the changes within the alloy composition towards the corroded surface areas, a series of element distribution curves, measured from the centre of the sample to the edge of the corrosion layer, was created, as well as element distribution charts (elemental maps).

The second group of artefacts—those from NBA III sites in Mecklenburg—were visually analysed with an eye to studying the remaining traces left from the crafting process. The result is a superficial knowledge of the traces left by different tools, techniques and habits of the craftsperson during the production process (i.e. Nørgaard 2015c). When this knowledge is compared to the deformations, or non-deformation, of the metal's microstructure as is documented within the metallographic examination, it is possible to create a detailed operational sequence of the artefacts' production. In addition, several scientific investigations were executed in order to answer the initial question posed at the start of this discussion as to the nature of specific individual alloys. The Archäologisches Landesmuseum Mecklenburg-Vorpommern restricts examination of its collection to non-destructive methods; thus, the analysis of those objects in the sample from the Mecklenburg region was executed using a handheld energy-dispersive XRF spectrometer (Niton X13t GOLDD) to reveal their trace element composition. A handheld XRF spectrometer measures and analyses the metal composition of an artefact near the surface. It is based on the principle that an X-ray photon, emitted from an X-ray tube, removes an electron from the inner shell of an atom (for a more detailed description of the process, see Anker 1982, Helfert & Böhme 2010, Wolff 2009). Thus, it measures the elemental composition of the sample's surface. As was indicated in the earlier case study, the results are strongly influenced by the effects of corrosion on the distribution of elements at an object's surface.

3 Results and Discussion

Most of the Scandinavian and north German bronzes considered here were found in agricultural areas or bogs, and, due to a similar climate and agricultural practices, have been exposed to similar conditions. Therefore, the corrosion documented through the metallographic investigation of the bronze ornaments from Lower Saxony is comparable to that visible on the ornaments from Mecklenburg. As such, the destructive (metallographic) analysis of the artefacts from Lower Saxony can be used to understand the results from the non-destructive analysis of the artefacts from Mecklenburg.

¹ For more information concerning the crafting of NBA II-III ornaments see Nørgaard 2014; 2015c.

3.1 Some Specific Information on Corrosion

The majority of bronzes dated to 1500–1300 BC are Cu-Sn alloys (tin bronzes), which, when exposed to moist air under pre-industrial conditions, develops a patina consisting largely of basic copper (CuCO $_3$). These CU (II) salts can differ according to the deposition context of the bronze artefacts, e.g. malachite (Cu $_2$ (CO $_3$)(OH) $_2$) when corroded in soil, brochantite (Cu $_4$ (SO $_4$)(OH) $_6$) when exposed to the atmosphere, or atacamite (Cu $_2$ Cl(OH) $_3$) when placed in seawater. They commonly cover a red cuprous oxide (Cu $_2$ O; SnO $_2$) layer (Bernard & Joiret 2009, 5200, Constantinides et al. 2002, Robbiola et al. 1998, 2084). Therefore, the monoclinic emerald-green to blackish carbonate and the glaze blue azurite, which develops into the familiar greenish malachite (Mircea et al. 2012, 180, Wolters 1991, 206), dominates the appearance of the bronze artefacts. Consequently, the appearance of carbon (C) and oxygen (O) as primary and secondary chemical compounds is of particular importance for the understanding of the corrosion layer. In addition to oxygen, chlorine (Cl) is also detected in almost all corrosion layers. As Oudbashi and colleagues (2013) point out, the presence of chlorine in the burial environment of an artefact causes a reaction with its copper and a formation of cuprous chloride. In the worst case, such exposure can lead to what is known as 'bronze disease'—a 'reaction of copper with chlorine in presence of moisture and oxygen that causes the formation of copper trihydroxichlorides ... until all metallic copper converts' (Oudbashi et al. 2013, 8).

Furthermore, minor elements contained in the soil can influence the composition of the corrosion layer. The metals contained in the immediate area around the deposited bronzes can accumulate in the corrosion, in particular manganese and cobalt, as well as phosphorus and silicon, which appear frequently in modern soil due to the effects of modern agricultural work. Thus, it can create a concentration of secondary metals, including iron (Fernandes et al. 2013, 4, Pernicka 1995, 44) and aluminum (Mircea et al. 2012, 183).

Robbiola and colleagues (1998), as well as Chase (1994), have suggested that ion migration is responsible for the observed effects within the corrosion layer. In order to explain the formation of copperalloy patinas, they have classified corrosion structures according to several types. The Type-I structure an even surface with a two-layer structure incorporating internal tin oxidation accompanied by selective dissolution of copper—is characteristic for quaternary bronze (CU-Sn-Zn-Pb) and brass (Cu-Zn) (Robbiola et al. 1998, 2090, Constantinides et al. 2002, 92). It also appears on tin-bronzes (Cu-Sn) as 'noble patina'. The Type-II structure—a coarse three-layered structure with a general uneven structure and corrosion attacks such as pitting—appears frequently on arsenical bronzes (Cu-As), tin bronzes (Cu-Sn) and leaded bronzes (Cu-Sn-Pb) (see Robbiola et al. 1998, 2097, Constantinides et al. 2002, 93-95). Interestingly, with an average thickness of 25-34µm and a minimum thickness of 3µm the Type-I corrosion layers are much less developed than the Type-II corrosion layers of tin bronzes (Cu-Sn). The average thickness of the latter measures 67µm (measured on artificially-produced patina, table. 1). Furthermore, Constantinides and colleagues observed an aggressive corrosion process in tin-bronzes at places 'where the original surface is destroyed' (Constantinides et al. 2002, 93); however, such developments are advantageous in craft technical studies, as punch marks, intensive hammering of the surface, or inserted decoration would be visible within the corrosion layer. This visibility of decorations applied post casting could be supported by the metallographic analysis of the bronze ornaments from Lower Saxony (Nørgaard 2015b, 121).

Table 1. The thickness of the corrosion layer in regard to the type of copper-alloy (based on Constantinides et al. 2002, 100).

Composition	Range of	Average of	Туре
	thickness (µm)	thickness (µm)	(after Robbiola 1998)
Quaternary bronze	14-146	34	I/ Pit
Arsenical copper	23-78	38	II/ Pit
Tin bronze	40-138	67	II
Leaded tin bronze	18-60	25	I /II/ laminated
Brass	3-73	24	1

3.2 Differences in Element Composition Between Surface and Metallic Core

Results from the SEM analysis of the bronze ornaments from central Lower Saxony outlined here mark an important contribution to ongoing discussion regarding handheld XRF analysis of museum collections.

Initial visual, qualitative analysis of thin sections taken from samples of most artefacts considered revealed advanced corrosion (see figure 1). Occasionally it is to be inferred that no metallic core material is left as the artefact is brittle and very light, which is characteristic of fully corroded bronze (Oudbashi et al. 2013). To gain more information about the corrosion crust, an element distribution curve was charted for several samples displaying a full cross-section and a sample thickness of 1-2 mm, tracing changes in composition from the sample's centre to the edge of its corrosion layer. The curve depicting element distribution for the neck collar from Luttmissen, in Lower Saxony², for example, showed a rapid drop of the copper values, as well as a simultaneous and disproportionate increase in tin content with the transition to the corrosion layer (figure 1).

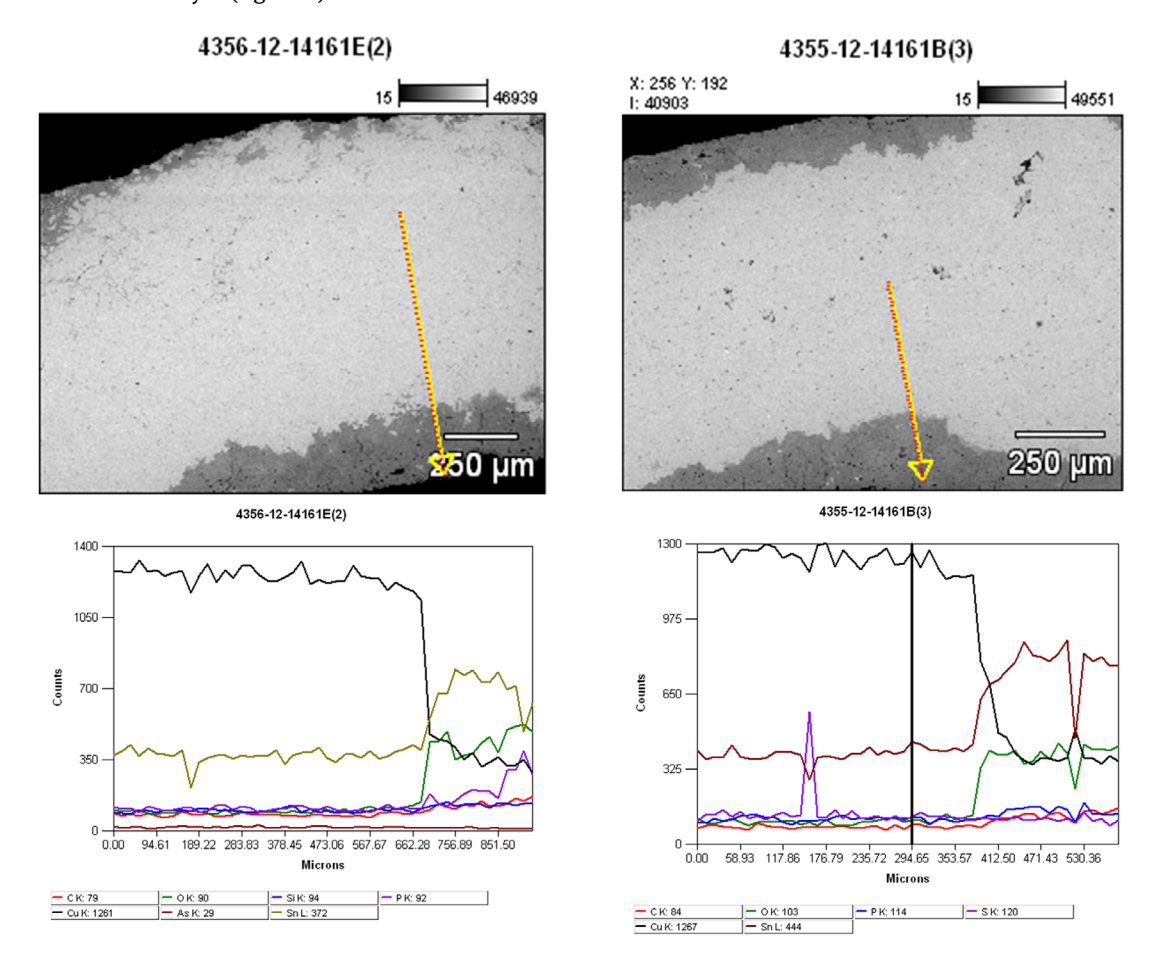


Figure 1. SEM analysis of the specimen sample from the front section and the end plate of the neck collar from Luttmissen, Uelzen (LMN 14161). The element curve clearly shows the change in the elemental values (scan: Dirk Kirchner, German Mining Museum, Bochum).

Similar phenomena have already been documented in other studies of ancient bronzes, mostly within conservation studies, while comparable results have been achieved in studies of artificially-created patinas

² Two samples were taken from the neck collar found in Luttmissen, Uelzen, Lower Saxony LMH14161 (Laux 1971); - one from the ribbed section and one from the end-plate.

(Fernandes et al. 2013, 5, Oudbashi et al. 2013, 3, Šatović et al. 2013, Constantinides et al. 2002, 93ff.). Copper dissolution, which starts with selective dissolution from the copper solid solution α -phase (see Robbiola et al. 1998, 2108), is commonly known as 'decuprification'. During this stage, the dissolved copper reacts with soil anions such as chloride (Cl) and carbon (C), and as these copper salts are soluble in soil waters, they can be carried away from the metal surface (see Chase 1994, Oudbashi et al. 2013, Weisser 1975). Along with the decrease in the copper values, the oxygen content rises sharply. This effect results from the reaction of copper and oxide to the copper-oxide cuprite.

Since tin reacts to a much lesser extent with oxygen, the percentage of tin content in the alloy is not changed; in fact, the additional enrichment of tin in the corrosion layer (Pernicka 1995, 44) results in a distinct increase in its proportion relative to other components. In several studies of bronze corrosion, a high tin concentration has been detected in corrosion layers. Selective de-alloying, or 'destannification', from the bulk metal (and the tin rich δ -phase) towards the corrosion provides one possible explanation for this phenomenon, while selective removal of tin offers an alternative (see for example Chase 1994, Weisser 1975). In this case, the fast oxidation of tin can be seen as the main motivation for its dissolution from the bulk (tin-oxide films); however, this phenomenon requires further investigation.

With respect to the two alloying components of tin-bronze, copper and tin, one can speak of a disproportionate reversal of their percentages within the corrosion. However, within three-layered Type-II-corrosion crusts, the chemical composition changes greatly from one layer to the next (Robbiola et al. 1998, 2101).

Element distribution maps (figures 2 and 3) demonstrate that the sharp rise in oxygen content, as well as the dissolution of copper and tin, are not local phenomena.

Figure 2, captured using the SEM, depicts half the cross-section of a sample taken from a neck collar's end plate³. Clearly, the uneven corrosion layer (Type I/II corrosion, Robbiola et al. 1998, 2099) of about 30µm is visible, as is the protruding corrosion at the grain boundaries. The SEM allows filtering of specific elements, therefore it possible to visualise solely the distribution of, for example, oxygen and copper (figure 2, O K and Cu K – K indicates the shell) in an elemental map. These maps demonstrate that the decrease of copper within the corrosion is correlated to an increase in oxygen, and that this phenomenon occurs consistently throughout the corrosion. Additionally, the proportion of carbon (figure 2, C K) increases in the corrosion crust. One can infer that the decrease in copper is part of the decuprification process⁴. Simultaneously, tin becomes more densely concentrated (figure 2, Sn L).

The minor trace elements contained within the alloy also exhibit changes that are caused by the corrosion process. Sulphur inclusions were found in the vast majority of the metallographically-examined bronzes from the Lüneburg Heath (see Nørgaard 2014a, 2015b). The detectable percentage of the sulphur content in most samples was constant; however, a slight increase in the sulphur values could be detected within the corrosion layer. Arsenic could be only sporadically documented in the samples (figure 3, As K). It is striking, however, that in the samples considered here, although arsenic-containing inclusions predominantly occured at the transition to the corrosion layer, they could not be detected at the outer edge of the sample (figure 4).

Changes in alloy composition within the corrosion crust were documented for all samples examined (figure 5). Depending on the type of corrosion (both Type-I and Type-II structures were present) the composition changed once or twice (for three-layered structures, see figure 5, 4931(6)). However, the investigation led to some unexpected results.

A specimen sample from the site labeled as 'Lüneburgisch' provides a particularly interesting case. The fragment of a neck collar endplate with vertical ribbing and undecorated ends (see Nørgaard 2011, 34-35), examined under the SEM, showed a coating/layer with a dense structure, apparently attached to the original surface of the artefact (figure 6). According to its element distribution curve, the artefact shows a familiar shift in the copper and tin values in the transition from bulk metal to the corrosion crust. However, in the transitional area, the proportion of copper increases drastically (from 38.37 to 72.18 weight %, see figure 6)

³ Neck collar from Raven, Harburg, Lower Saxony (LMH 4932).

⁴ However, some of the measured C in the elemental curve might be a reflection of the surrounding epoxy resin.

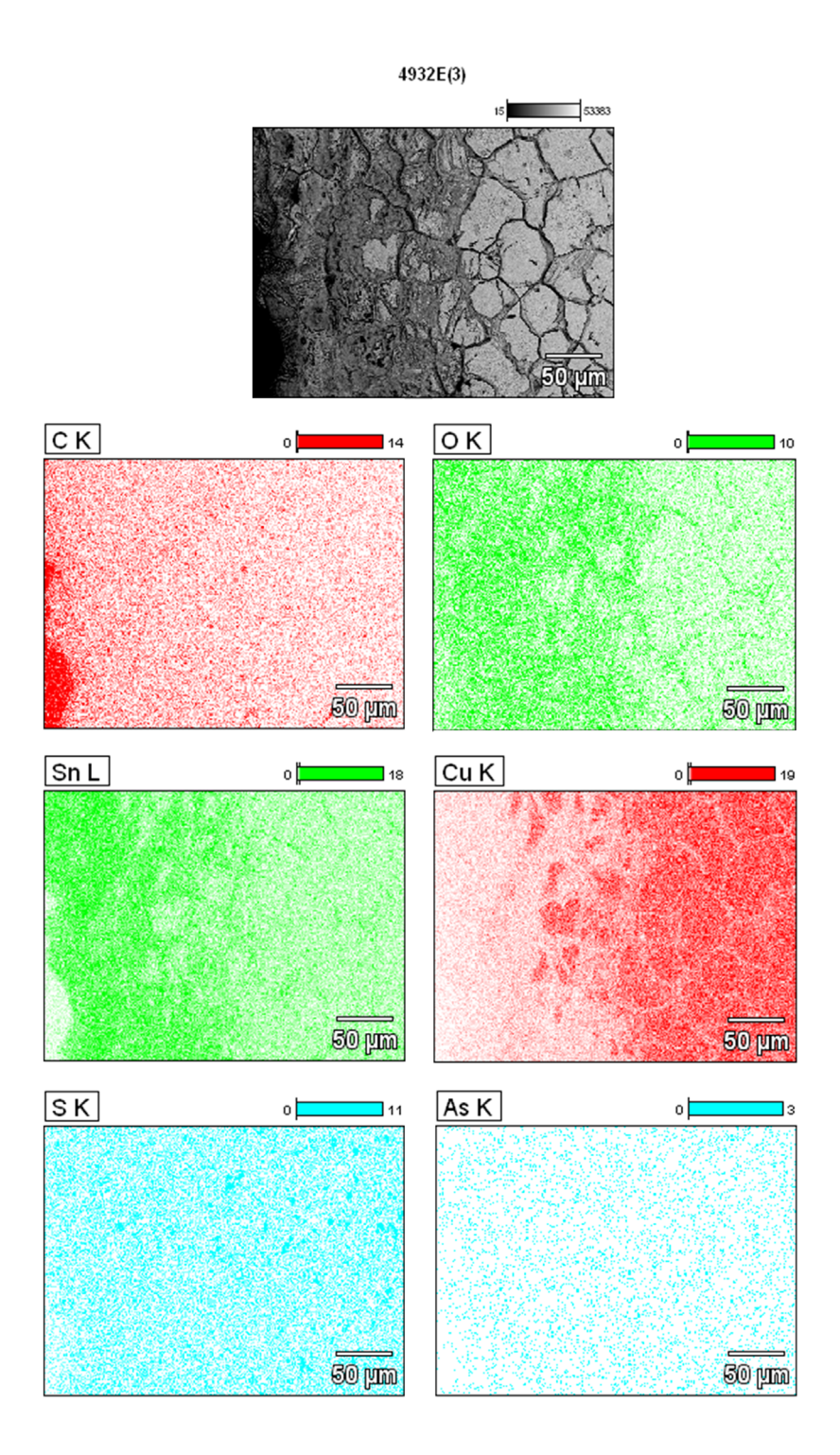


Figure 2. Elemental map of the alloy components from the sample of the neck collar from Raven, Kr. Harburg, Lower Saxony (LMN 4932). The sample is taken of the end plate of the collar (scan: Dirk Kirchner, German Mining Museum, Bochum).

and the tin proportion falls below its original value (figure 6 and 7). Additionally, sulphur content reaches its peak at the transition to the coating. This phenomenon becomes apparent in mapping the distribution of these elements. Both the distribution of copper (Cu) and tin (Sn) within the sample indicate a coating, as does the linear concentration of sulphur (S) along the surface of the artefact (figure 8). The appearance of tin, arsenic, and iron in the coating layer prompts one to question what this coating was made of and how it may have come to be present on the surface of such artefacts.

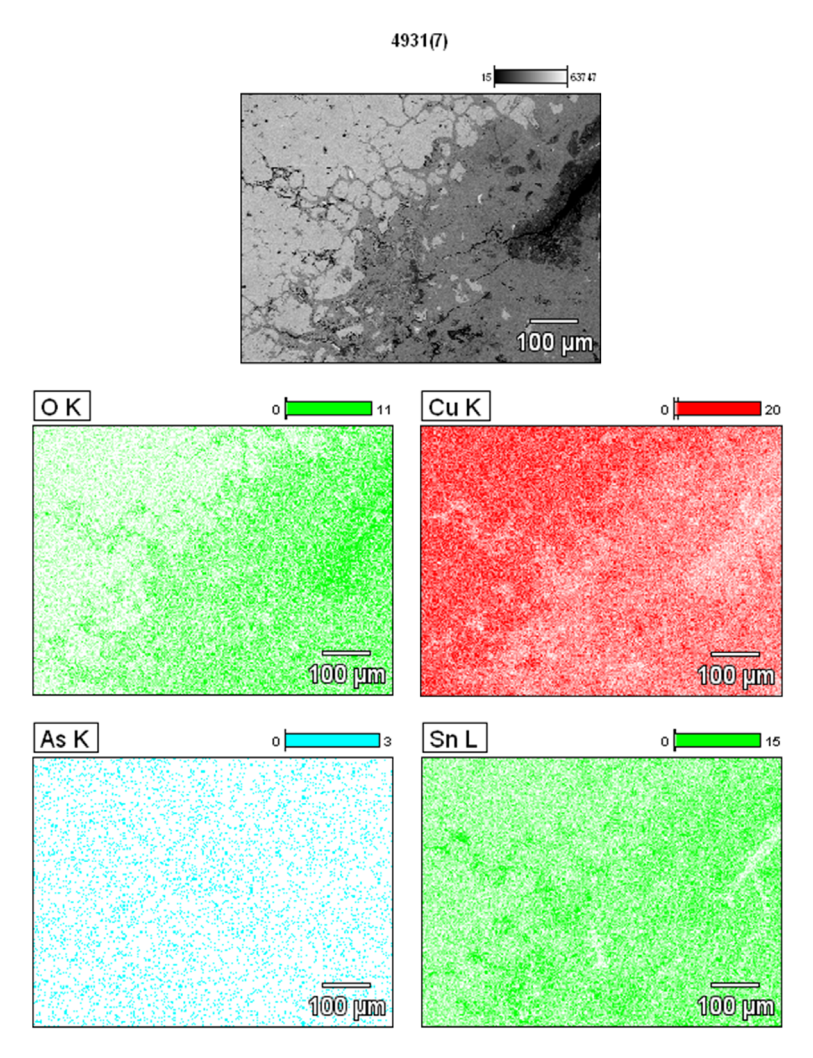
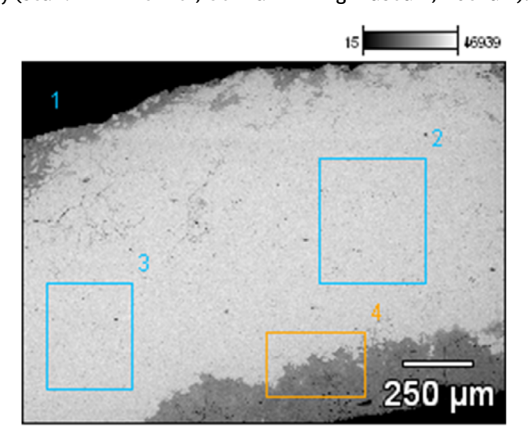


Figure 3. Elemental map of the alloy components from the sample of the neck collar (LMN 4931) from Rehlingen, Lüneburg, Lower Saxony (scan: Dirk Kirchner, German Mining Museum, Bochum).



	C-K	О-К	Si-K	P-K	S-K	Си-К	As-K	Sn-L
14161E_pt1	53.37	31.95				11.89		2.80
14161E pt2					0.38	86.07		13.55
14161E_pt3					0.24	85.17		14.59
14161E pt4	5.81	17.10	0.65	0.32		51.84	0.46	23.82

Figure 4. SEM analysis of the specimen sample from the end plate of the neck collar from Luttmissen, Uelzen (LMN 14161). The table lists the measured values of the individual measurements 1-4 (scan: Dirk Kirchner, German Mining Museum, Bochum).

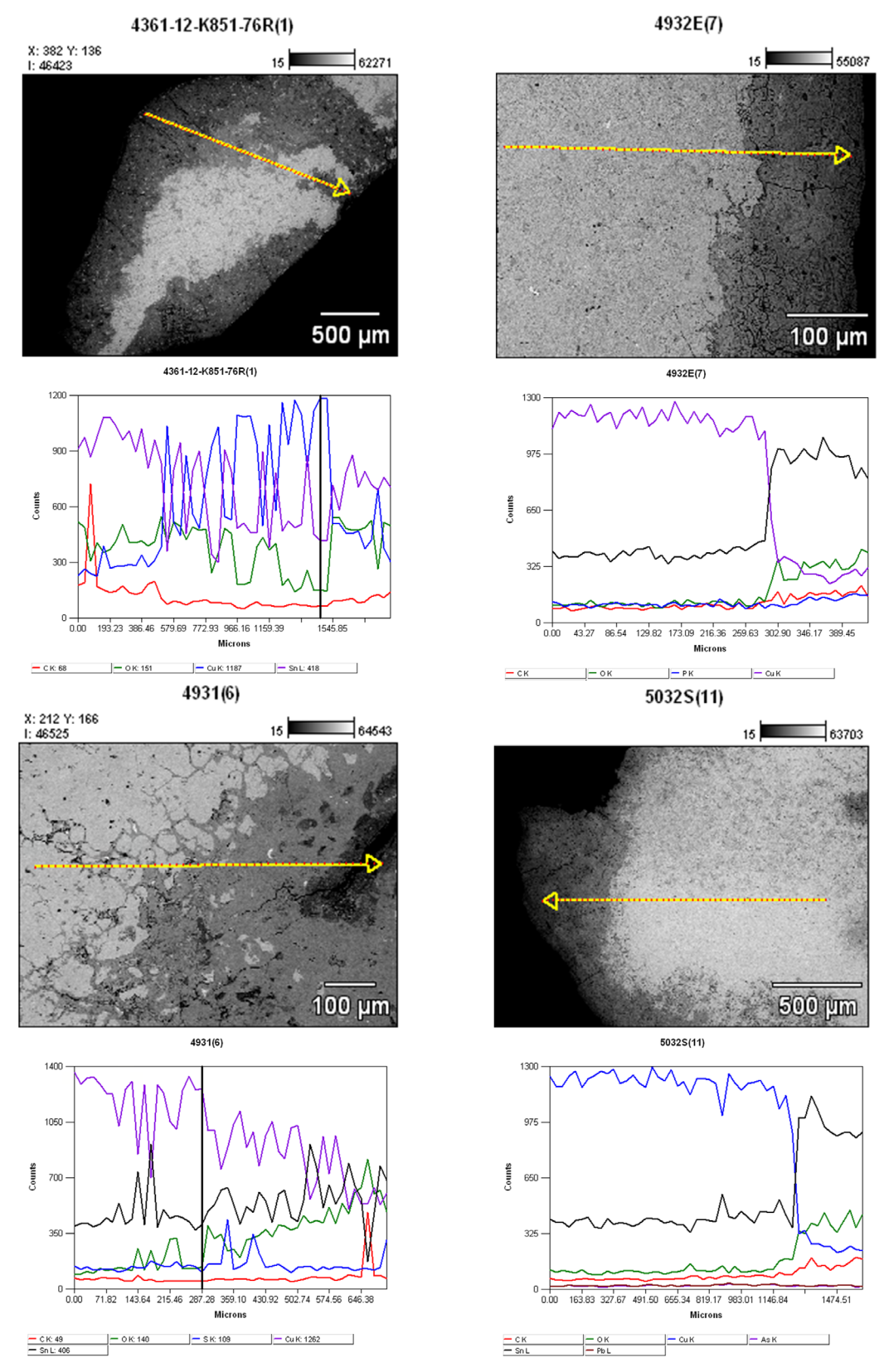


Figure 5. Elemental curve from several samples taken for metallographic analyses. Top left, Bleckmar, Celle, Lower Saxony (LMN K851:76); Top right, end part of the collar from Raven, Kr. Harburg, Lower Saxony (LMN 4932); Left, Rehlingen, Lüneburg, Lower Saxony (LMN 4931); Right, shaft of the pin (LMN 5032) from Rehlingen, Lüneburg, Lower Saxony (scan: Dirk Kirchner, German Mining Museum, Bochum).

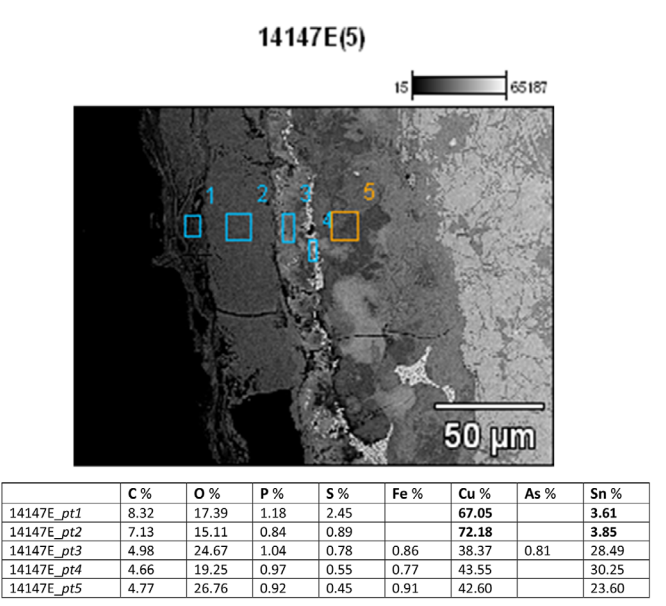


Figure 6. Specimen sample from the end part of the collar near Lüneburg (LMN 14147). The SEM data clearly show a severe element composition at the outer layer of the collar (scan: Dirk Kirchner, German Mining Museum, Bochum).

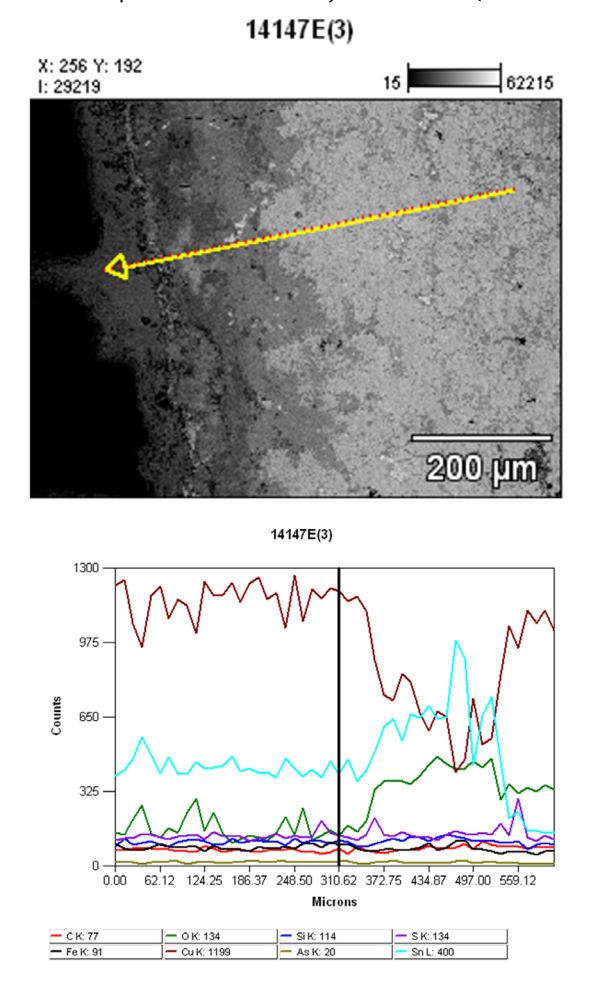


Figure 7. SEM analysis and elemental distribution curve of the specimen sample from the collar (LMN 14147) near Lüneburg (scan: Dirk Kirchner, German Mining Museum, Bochum).

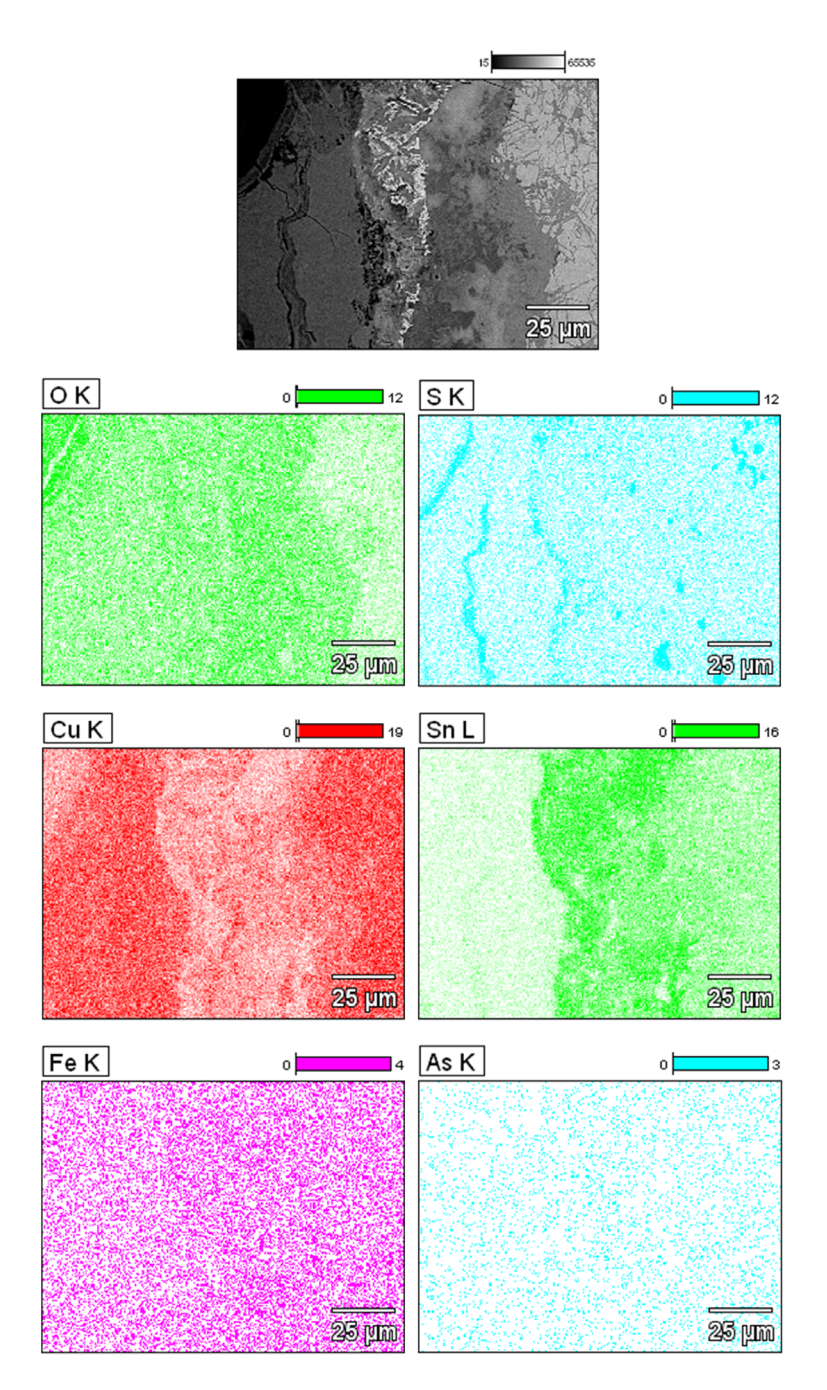


Figure 8. Elemental distribution map, with arsenic and iron, of the specimen sample from the collar (LMN 14147) near Lüneburg (scan: Dirk Kirchner, German Mining Museum, Bochum).

For restoration purposes as well as to imitate a green antique patina, linseed oil varnish, mixed with malachite or azurite, has historically been used. Such treatment was especially popular at the end of the nineteenth century (Copper Development Association 2008, Groves 2001). Occasionally, powdered copperalloy material was also added to the varnish. It can be assumed that the coating detected on this artefact is such a varnish and that it was applied to give the neck collar the 'typical green colour' of Bronze Age artefacts for its exhibition. Alternatively, it is possible that this layer was added as a conservational measure, as it has obviously limited the effects of corrosion of the artefact's surface.

Thus, the analysis conducted here of thin sections from artefacts of the Lower Saxony region allows one to conclude that that the metal composition of an object's surface does not reflect the composition intended by prehistoric artisans.

3.3 The Limits of Non-Destructive XRF Analysis on Archaeological Bronzes

Examination under the SEM clearly showed a marked change in the trace element composition from the core to the corroded surface of the bronzes. This observation leads one to infer that studies of corroded artefacts using a handheld XRF will not allow for the characterisation of the original alloy.

In order to determine a deterioration of the results by such corrosion layers in the bronzes, comparable data was assembled using portable XRF devices from two fragments of identical bracelets, found within an urn from the tomb of Gielow⁵ (ALM IV/64/561 c and d) and now held in the National Museum of Mecklenburg (see also Nørgaard 2015a). A quarter of each fragment was cleansed of the patina, which covers the remaining surface (figure 9). Two readings were taken for each artefact—one at the patina, and another from the polished area. A comparison of the two measurements revealed the corroded area to contain 3-4% less copper than the polished area, with an increased tin value of up to 4%. Furthermore, a slight deviation was recognisable in regard to the further elements such as arsenic, which was present in usually a few tenths or hundredths of the values observed for the polished areas.

IV/64/561c	Cu%	Sn%	Pb%	Ag%	As%	Au%	Bi%	Co%	Fe%	Ni%	Sb%	Zn%	P%	Si%	Ti%	Zr%	Nb%
polished	85,67	11,27	0,22	/	0,170	1	/	0,025	0,157	0,394	0,091	0,130	/	1,50	0,091	0,015	0,004
corroded	81,68	12,24	0,17	/	0,233	1	1	0,022	0,113	0,492	0,107	0,131	1,22	2,80	1	1	/



Figure 9. Bracelet from Gielow, Kr. Malchin in Mecklenburg. Using the XRF device, once the polished section and the corroded section of the bracelet were measured (picture: Heide Wrobel Nørgaard).

However, as the thickness, as well as the properties, of the corrosion layer (see figure 5, K851) can differ from artefact to artefact (Type-I corrosion and Type-II corrosion appear on artefacts with similar alloy components), it is therefore not appropriate to value the deviation of tin and copper to around 4%.

Detailed study of the element distribution curves (see figure 5) clearly demonstrates the impact of corrosion on the distribution of elements. As is shown by the data measured from the corroded artefacts in Mecklenburg (table 2)⁶, variations within the proportional values for tin are massive. Based on a variety of

⁵ Gielow, Kreis Malchin, Mecklenburg (Schoknecht 1965, 109, Nørgaard 2011, 62-64).

 $[{]f 6}~$ See also supplementary material: extended table 2.

archaeological and archaeometallurgical studies of north German Bronze Age material culture, one might expect the artefacts investigated here to contain tin in proportions of between 8-12%, and possibly up to 14%. Data obtained via SEM from the artefacts from Lower Saxony support such a conclusion (see table 3). As such, values between 8.71 to 55.56% obtained via handheld XRF illustrate a severe difference. Commonly, within the earliest Bronze Age, artefacts were made of relatively pure copper or a multi-impurity metal with high levels of nickel and antimony (for further reading, see i.e. Junghans, Sangmeister, & Schröder 1974, Sangmeister 1971). During the early and middle Bronze Age in north Germany, copper-tin alloys were prevalent. The proportional presence of tin varies from 9-12% in NBA II and from 8-11% in NBA III⁷. Occasionally, artefacts contained 13-17% tin, as this composition was fairly widespread during the Taunton phase in the British Isles (i.e. Harding 2000, 204). As trading relations between these regions are known to have existed, one might assume the recycling of materials took place. However, only twenty of the seventytwo artefacts from Mecklenburg analysed for this study were determined to be close to these common compositional values.

The data leads one to conclude that the artefacts considered here are not equally well preserved. A superficial examination of their surfaces and accessible cross-sections could indicate the extent of their corrosion (as also shown in table 2); however, the data differs greatly from the compositions that were expected. A range of minor elements were measured, including aluminum (Al), manganese (Mn), phosphorus (P), and silicon (Si). As the X-ray penetration depth is limited to 100-200µm (Šatović et al. 2013, 7), these elements clearly were not a component within the original alloys; rather, they likely migrated from the soil into the developing corrosion layers. Still, the presence of such elements can provide useful data, informing the conservator of the degree to which the corrosion crust is developed, while determining the value of a visual, qualitative assessment of the state of corrosion.

The data from Mecklenburg was experimentally used to execute some calculations in order to consider the question of material groups related to Bronze Age workshops. To this end, proportional values obtained for those elements clearly related to the corrosion process (like Al, Cd, Cr, Mn, Mo, Nb, P, Si, Ti, V, W or Zr) were added and the total subtracted from 100%. In order to achieve a comparable composition of solely original alloy elements, the remaining elements were proportionally extrapolated to 100% (see table 4). At first sight, some of these calculated (in the sense of being mathematically constructed) compositions could be used in further evaluations of the material. Not knowing the original data, over 50% of the calculated elemental composition of the artefacts matches copper-tin (Cu-Sn) bronzes that could well have been present during the Bronze Age. However, they are calculated and, as such, are not necessarily indicative of the original alloy. None of these bronzes were examined if a metal core was still present. Some bronzes might have just a few µm of corrosion crust while others might have up to 1mm. As shown in table 4, a large number of artefacts contained tin in proportions far greater than their likely composition at the time of production. The uncertainty of the estimated data is also visible in the serious deviation of the tin content, ranging from 9.5% to 64%. Furthermore, the unreliability concerning the patina type, as suggested within this study, is striking.

As a result, analysis of metal composition using a non-destructive XRF device is not suitable to discussions related to the fine qualities of alloys used by contemporary craftspeople. The data also made clear that even when the material consists of artefacts in superficially similar corrosive conditions, one can find significant variation in elemental composition and depth of corrosion. As comparative studies have shown, bronzes with 'noble patina' (type I patina) and a high lead content might be better suited for such investigations (e.g. Fernandes et al. 2013, Šatović et al. 2013).

⁷ It should be noted that this information derives mainly from the analysis of weapons (axes) or ingots (see Junghans, Sangmeister, & Schröder 1974). It might be possible that ornaments contain a slightly higher tin percentage as has also been seen within the analysis of the ornaments from Lower Saxony.

Table 2. The data measured by the XRF device on the artefacts from Mecklenburg (German Mining Museum, Bochum). In order to compare the measurements, the patina type is given based on a superficial examination (including visible profile sections) of the artefacts. Additional, the major corrosion elements are given in values, the less frequent elements are named (< indicates a measurement below the detection limit of the device of around 50ppm).

												•			
ID location	sample position	patina*	Cu in %	Sn in %	Pb in %	As in %	iN ii %	Bi in %	Sb in %	Zn in %	Fe in %	Al % ni %	P ii	Si in %	
191 Gielow, MSE	arm ring, polished part	removed 85.67	85.67	11.27	0.22	0.17	0.394	,	0.091	0.13	0.157			1.5	Nb/Ti/Zr
193 Gielow, MSE	arm ring, polished part	removed 84.66	84.66	11.46	0.11	0.299	0.705	~	0.139	0.083	0.118			1.97	F
199 Mecklenburg	neck collar, end	removed	84.66	13.83	0.13	0.33	0.376	0.009	0.088	0.107	0.045				Ti/Zr
224 Bütow, MSE	neck collar, profile	type I	83.71	11.55	0.02	0.194	0.377	~	0.381	~	0.177			2.6	ij
262 Bütow, MSE	neck collar, inside	type I	84.84	11.83	0.09	0.2	0.421	~	0.389	~	0.146			1.58	Ę
192 Gielow, MSE	arm ring, inside	type I	81.68	12.24	0.17	0.233	0.492	~	0.107	0.131	0.113		1.22	2.8	
194 Gielow, MSE	arm ring, inside	type I	81.27	14.31	0.13	0.38	0.624	~	0.177	0.101	0.075		0.47	2.04	
238 Heinrichswalde, MSE	disc head pin, head	type I	89.98	9.25	0.77	0.199	0.214	~	~	0.048	0.464			0.62	Ti/Zr
263 Lubmin, VPG	neck collar, inside	type l	38.48	49.36	0.15	0.218	~	0.025	~	0.147	8609		0.71	3.4	=
264 Lubmin, VPG	neck collar, front	type I	34.02	46.4	0.14	0.173	~	0.022	~	0.118	2778	8.52	1.14	5.99	Ti/W
195 Mecklenburg	neck collar, front	type I	79.98	15.16	0.16	0.198	0.275	~	0.047	0.112	0.049		0.67	2.98	Ti/Zr
198 Mecklenburg	neck collar	type I	80.83	13.72	0.17	0.377	0.344	0.013	0.07	0.093	0.114			2.76	Ti/Zr
203 Mecklenburg	neck collar, triangle piece	type I	41.56	42.28	1.57	0.549	0.087	0.075	~	0.134	0.592	5.13	2.19	4.97	TI/W
289 Mecklenburg	neck collar, triangle inside	type I	37.37	47.73	1.74	0.549	0.092	0.087	~	0.114	0.75		2.06	5.4	TI/W
219 Mecklenburg	neck collar, inside	type I	77.29	18.35	0.41	0.219	0.147	0.013	0.038	0.137	0.216		1.55	1.26	W/Zr
220 Mecklenburg	neck collar, front	type I	68.79	23.96	0.61	0.397	0.385	0.032	0.064	0.212	0.183		3.44	1.28	Ti/W
256 Mecklenburg	neck collar, end	type l	62.02	31.37	0.49	0.251	0.242	0.03	0.063	0.122	0.325		2.59	1.44	8
257 Mecklenburg	neck collar, front rib	type l	69.24	24.76	0.59	0.411	0.226	0.036	90.0	0.199	0.288		2.23	1.4	Ti/W
258 Mecklenburg	neck collar, front decor	type I	69.02	22.36	0.57	0.352	0.306	0.023	0.053	0.188	0.143		2.46	1.23	≔
226 Mecklenburg	neck collar, front	type I	66.16	19.41	1.05	0.445	0.458	0.081	0.154	0.134	0.488		1.2	8.64	;
200 Möllen, LRO (GÜ)	neck collar	type I	78.32	16.26	0.2	0.271	0.137	~	~	0.125	1223			2.99	; =
197 Pisede, MSE	neck collar, inside	type I	81.32	12.89	0.48	0.315	0.62	0.026	0.126	0.184	0.079		1.34	1.47	Ti/Zr
265 Pisede MSF	neck collar, front decor	type I	79.99	13.96	0.52	0.326	99.0	0.032	0.107	0.158	0.064		1.2	1 56	F

metal												major c	major corrosion elements	elemen	ts
ID location	sample position	;	 3 .		 a ; a ;				Sb .	Zn	e	 ¥ .	 a :	Si .	
		patina*	% ui	ui %	% ui	in %	i % ui	ui %	% ui	% ui	% ui	% ui	% ui	"ui	
215 Poltnitz, LUP	leg ring, inside ring	type I	83.35	11.48	0.16	0.19	0.346	V	~	0.124	0.317		1.08	1.34	Mn/Ti/V/Zr
233 Poltnitz, LUP	armring, fragment	typeI	71.81	8.88	0.32	0.1	0.463 <	v	~	0.049	0.42	96.8	4.7	3.19	Mn/Ti/V
252 Poltnitz, LUP	leg ring, inside ring	typeI	83.59	9.34	0.3	0.295	0.52 (0.013	0.497	0.149	0.151		1.52	1.46	Mn/Nb/Ti/V/Zr
261 Poltnitz, LUP	armring, fragment	type I	82.93	10.01	~	0.297	> 998.0	~	990.0	~	0.36		2.76	1.81	Ti/V
211 Sparow, MSE	disc head pin	type I	81.76	14.53 (0.26	0.337	0.518 (0.014	0.11	0.1	0.189		0.81	0.93	⊢
213 Wotenitz, NWM	neck collar, inside	type I	22.01	44.43	~	0.529	0.148 <	V	~	0.131	22352		0.48	7.96	Mn/Ti
214 Wotenitz, NWM	neck collar, front	type I	21.29	45.87	0.01	0.548	0.17	V	~	0.152	21059		0.53	9.08	Mn/Ti/W/Zr
253 Wotenitz, NWM	neck collar, less patina	type I	47.23	29.98	~	0.392	0.224	v		0.205	11119		0.24	8.58	Mn/Ti
221 Alt Sammit, LRO (GÜ)	neck collar, front	type I+	65.55	23.96 (8.0	0.625	0.351 (0.045	0.198	0.22	0.405		3.1	4.01	Mo/Ti
259 Alt Sammit, LRO (GÜ)	neck collar, inside	type I+	89.99	21.5	0.84	0.514 (0.351 (0.039	0.201	0.221	0.432		2.88	5.64	<u> </u>
201 Alt Sammit, LRO (GÜ)	neck collar, coating	type I+	28	29.52	1.11	0.691	0.442 (0.048	0.223	0.323	0.933		2.68	3.1	Ti/W
231 Karbow, LUP	disc head pin, head	type I+	76.67	9.45 (0.27	0.15	0.384 <	~	0.062	0.124	0.738			7.12	Mn/Ti/V/Zr
235 Lubmin, VPG	neck collar, coating	type I+	35.96	40.67	0.15	0.209	·	0.022	~	0.123	7728	97.9	0.89	8.9	□
242 Thürkow, LRO (GÜ)	neck collar, inside	type I+	51.63	39.46	1.07	0.462	0.328 (0.071	0.092	0.078	3022		1.34	1.87	
243 Thürkow, LRO (GÜ)	neck collar, front/end	type I+	41.9	43.56	1.14	0.483	0.682 (0.068	0.131	0.158	2124		3.35	3.58	ī
208 Alt Sammit, LRO (GÜ)	ring knive, tip	type I-II	31.91	32.19	31.23	~	0.224 <	~	0.826	1.65	0.18				
209 Alt Sammit, LRO (GÜ)	ring knive, centre	type I-II	54.08	32.99 (29.0	0.888	0.673 (0.042	0.162	0.352	0.216		3.97	2.49	Ti/W
244 Amt Grabow (Wittenmoor),	neck collar, front	type I-II	58.32	23.35	1.33	0.521	0.423 (0.057	~	0.21	0.284	7.15	4.6	2.85	ij
293 Amt Grabow (Wittenmoor), neck collar, inside	neck collar, inside	type I-II	50.49	23.83	1.35	0.37	0.17 (0.054	~	0.162	0.457		5.32		Ti/V/W
232 Dabel, LUP (PCH)	belt disc	type I-II	82.06	13.96 (0.23	0.335	0.281 <	.,	0.149	0.075	0.238			2.31	
212 Karbow, LUP	neck collar, inside	type I-II	78.8	14.85 (0.18	0.316	0.31	.,	~	0.148	0.099		2.21	1.32	Ti/Zr
247 Lübz, LUP	neck collar, outside	type I-II	81.61	12.93 (0.61	0.089	0.167 (0.024	0.4	0.115	0.042			2.83	Ti/W
248 Lübz, LUP	neck collar, inside	type I-II	82.53	12.95 (0.59	0.175 (0.327 (0.024	0.372	0.164	~			1.78	Ti/W/Zr
236 Poltnitz, LUP	neck collar, inside	type I-II	73.51	21.46 (0.04	0.089	> 60.0	· ·	~	0.152	0.772		1.33	1.46	Ti/W/Zr
237 Poltnitz, LUP	neck collar, decor	type I-II	73.45	22.45	0.04	0.073	0.084	,	~	0.115	0.998		1.25	96.0	Mn/Ti/W

metal												major	orrosior	major corrosion elements	ts
ID location	sample position	patina*	Cu in %	Sn in %	Pb in %	As in %	Ni in %	Bi in %	Sb in %	Zn in %	Fe in %	Al in %	P in %	Si in %	
249 Sparow, MSE	neck collar, inside	type I-II	73.83	19.98	0.42	0.518	0.618	0.016	0.182	0.115	0.115		2.21	1.37	Ti/W
250 Sparow, MSE	neck collar, front	type I-II	72.53	21.83	0.45	0.644	0.743	0.017	0.192	0.082	0.17		1.05	1.59	Ti/W
217 Wozinkel, LUP	neck collar, front decor	type I-II	75.96	16.69	0.38	0.615	1001	0.036	0.122	0.16	0.14		2.96	1.17	Ti/V
218 Wozinkel, LUP	neck collar, end	type I-II	75.18	16.89	0.32	0.634	0.859	0.035	0.113	0.152	0.227		1.78	2.07	Ti/V/Zr
210 Alt Sammit, LRO (GÜ)	ring knive , ring	type II	57.73	26.21	0.65	0.623	0.51	0.031	0.135	0.26	0.251		6.05	2.82	Ti/V
227 Amt Grabow, LUP	belt disc	type II	71.52	19.91	0.1	0.718	0.598	~	0.311	0.11	0.314		2.44	3.22	F
205 Boldebuck, LRO (GÜ)	neck collar, inside	type II	85.73	12.53	0.37	0.289	0.038	0.01	0.141	0.14	990.0				C
222 Bütow, MSE	neck collar, front	type II	56.53	26.23	0.03	0.367	0.343	~	0.677	0.131	1322	5.58	2.52	5.62	Ti/V/W
234 Friedrichsruhe, LUP	neck collar, fragment	type II	77.21	16.03	0.35	0.38	0.314	0.012	0.061	0.102	0.098		2.78	1.47	Mn/Ti/V
246 Kremmin, LUP	neck collar, inside	type II	68.51	10.71	0.19	0.112	0.145	0.014	0.041	0.062	0.379	4.8	1.22	13.21	Mn/Ti/Zr
286 Kremmin, LUP	neck collar, front	type II	96.99	8.78	0.18	0.106	0.222	0.008	~	0.072	0.381	6.58	1.87	14.42	Mn/Ti/Zr
287 Kremmin, LUP	neck collar, end	type II	67.07	8.71	0.24	0.115	0.147	0.009	0.031	0.058	0.517	3.81	1.32	17.48	Mn/Ti/W/Zr
202 Mecklenburg	neck collar, square piece	type II	33.54	55.56	0.05	0.064	0.081	~	~	0.111	0.897		3.87	2.62	Ti/V
290 Mecklenburg	neck collar, square centre	type II	34.11	56.21	0.05	90.0	0.063	~	~	0.113	0.92		3.79	1.86	Cd/Ti/V/W
239 Mecklenburg	neck collar	type II	76.25	11.76	0.02	0.03	0.038	~	~	0.108	0.825	5.5	2.78	1.59	Ti/V/Zr
291 Mecklenburg	neck collar, fragment	type II	75.8	18.7	0.03	0.111	0.126	~	~	0.137	0.05		1.95	2.54	Mn/Ti/V
196 Pisede, MSE	neck collar, front	type II	77.52	18.5	0.56	0.375	0.571	0.025	0.168	0.075	0.098		0.78	0.93	
204 Sarmstorf, LRO (GÜ)	neck collar, decor	type II	85.4	9.1	0.04	0.019	0.163	~	~	0.078	0.193			4.06	Mn/Zr
228 Turloff, LUP (PCH)	neck collar, inside	type II	84.1	13.75	0.3	0.07	90.0	~	0.049	0.082	0.072		0.55	89.0	Zr
229 Weisin, LUP	leg ring, inside ring	type II	68.09	27.79	1.72	0.436	0.252	0.023	0.168	0.116	0.352		2.08	2.25	Mn/Ti/V/W
230 Weisin, LUP	neck collar, inside	type II	82.83	12.68	0.14	0.084	0.063	~	~	~	0.134		0.73	2.98	
260 Gielow, MSE	neck collar, inside	type II+	80.8	11.86	0.31	0.071	0.131	0.024	0.087	0.258	1259			2.23	Mn/Ti/V/Zr
288 Mecklenburg	neck collar, end fragment	type III	29.55	57.23	1.67	0.462	0.15	980.0	~	0.117	1103	3.1	1.76	3.84	W
255 Wotenitz, NWM	neck collar, rim	type III	28.6	44.47	0.02	0.512	0.179	~	~	0.178	18138		0.34	5.85	Mn/Ti
		;													

+ additional unknown coating of artefact can have influence on the values * corrosion type suggested via surface and profile examination, type I-II has noble patina with occasional signs of pitting

Table 3: Elemental compositional data for the elements Cu, Sn and As, measured using a scanning electron microscope (German Mining Museum Bochum) on the bronze artefact from Lower Saxony (< indicates a measurement below the detection limit of 200ppm). For the complete dataset see Nørgaard 2015b, 122.

metal						
QI	mnsenm	location	date	Cu in %	Sn in %	As in %
4390	HLM 4390	Westerwevhe, Lüneburg, Lower Saxony	II-I 9Z	84.52	8.6	~
14145	HLM 14145	Edendorf, Ülzen, Lower Saxony	P II (?)	89.29	10.48	~
195:78	HLM 195:78	unknown location, Lower Saxony	P II (?)	88.45	11.13	~
13135bB	HLM 13135b	Becklingen, Celle, Lower Saxony	P.II	89.18	10.49	~
4931	HLM 4931	Rehlingen, Lüneburg, Lower Saxony	II-I 9Z	82.16	11.33	~
13135b E	HLM 13135b	Becklingen, Celle, Lower Saxony	P.II	88.00	11.54	~
12018 K	HLM 12018	? near Lüneburg/Westerweyhe, Lower Sa	Ы	87.09	11.79	0.65
14154	HLM 14154	Tangendorf, Harburg, Lower Saxony	ZG I-III	86.71	12.23	0.48
13178	HLM 13178	Amelinghausen, Lüneburg, Lower Saxony	ZG I-III	81.22	12.77	~
13135c	HLM 13135c	Becklingen, Celle, Lower Saxony	ВΠ	86.42	12.90	~
13135a	HLM 13135a	Becklingen, Celle, Lower Saxony	ЬΠ	85.53	13.47	0.32
13135a E	HLM 13135a	Becklingen, Celle, Lower Saxony	ВΠ	85.51	13.24	0.28
5032	HLM 5032	Rehlingen, Lüneburg, Lower Saxony	II-I 9Z	85.00	14.04	0.51
14148	HLM 14148	near Lüneburg, Lower Saxony	E II	84.49	14.21	0.81
14147	HLM 14147	near Lüneburg, Lower Saxony	P II (?)	84.33	14.29	0.81
14161 E	HLM 14161	Luttmissen, Ülzen, Lower Saxony	ВΠ	85.62	14.06	~
14161 B	HLM 14161	Luttmissen, Ülzen, Lower Saxony	ВΠ	84.94	14.85	~
14144/1	HLM 14144/ 1	Edendorf, Ülzen, Lower Saxony	P II (?)	84.66	14.88	~
14144/2	HLM 14144/ 2	Edendorf, Ülzen, Lower Saxony	P II (?)	85.22	14.33	~
4932 B	HLM 4932	Raven, Harburg, Lower Saxony	ZG III	84.94	14.41	90.0
4932 E	HLM 4932	Raven, Harburg, Lower Saxony	ZG III	84.71	14.69	0.11
5032 K	HLM 5032	Rehlingen, Lüneburg, Lower Saxony	II-I 9Z	84.78	14.59	~
99:33	HLM 99:33	Moorkathe, Fallingbostel, Lower Saxony	ЬΠ	80.52	15.19	~
13176	HLM 13176	Amelinghausen, Lüneburg, Lower Saxony	ZG I-III	84.14	15.20	0.27
14146	HLM 14146	near Lüneburg, Lower Saxony	P II (?)	83.43	15.92	~
13177 B	HLM 13177/ 13179	Amelinghausen, Lüneburg, Lower Saxony	ZG I-III	82.53	16.22	0.58
13177 B2	HLM 13179/ 13177	Amelinghausen, Lüneburg, Lower Saxony	JII-I 9Z	82.21	16.98	0.02
14147 E	HLM 14147	near Lüneburg, Lower Saxony	P II (?)	82.64	16.90	0.05

Table 4: Calculated average trace element composition of the artefacts from Mecklenburg. The elements related to the corrosion process are deducted and the resulting alloy relevant elements are proportional extrapolated to 100%.

metal														
QI	museum-number	additional information	patina*	Cu in %	Sn in %	Pb in %	As in %	Ni in %	Sb in %	Bi in %	Fe in %	Co in %	Zn in %	alloy in %
204	ALM Br.93	neck collar	type II	6.68	9.57	0.04	0.02	0.17	0	0	0.2	0	0.08	100
238	ALM 7236b	disc head pin	type l	88.8	9.47	0.78	0.2	0.22	0	0	0.48	0	0.05	100
233/261	ALM Br. 952a	average armring	type l	9.78	10.7	0.19	0.21	0.74	0.04	0	0.44	0.055	0.03	100
215/252	ALM Br. 954a	average legring	type l	87.47	10.9	0.24	0.25	0.45	0.26	0.005	0.24	0.02	0.14	100
231	ALM Br. 92	disc head pin	type I+	87.25	10.75	0.31	0.17	0.44	0.07	0	0.84	0.03	0.14	100
224/262	ALM Br. 1204	aver. neck collar profile	type l	86.7	12.02	0.05	0.2	0.41	0.4	0	0.165	0.04	0	100
246/286/287	ALM LIIQ, 4	average neck collar	type II	86.64	12.04	0.26	0.14	0.22	0.03	0.01	0.54	0.02	0.08	100
191/192	WA IV/64/561c	average armring	r/type l	86.55	12.17	0.2	0.2	0.46	0.1	0	0.14	0.02	0.13	100
230	ALM 2195	neck collar	type II	86.34	13.22	0.14	60.0	0.07	0	0	0.14	0	0	100
205	ALM Br. 271	neck collar, inside	type II	86.33	12.61	0.37	0.29	0.04	0.14	0.01	0.07	0	0.14	100
228	ALM Br. 371	neck collar, inside	type II	85.4	13.96	0.3	0.07	90.0	0.05	0	0.07	0	0.08	100
193/194	WA IV/64/561d	average armring	r/type l	85.22	13.24	0.12	0.35	89.0	0.16	0	0.1	0.02	60.0	100
260	WA IV/64/561b	neck collar	type II+	85.18	12.5	0.33	0.07	0.14	0.09	0.03	1.33	90.0	0.27	100
274/248	ALM 2000/1277, 3	average neck collar	type I-II	84.98	13.4	0.625	0.135	0.255	0.4	0.025	0.02	0.005	0.145	100
198/199	ALM S6	average neck collar	type l	84.71	14.11	0.15	0.35	0.37	80.0	0.01	0.08	0.03	0.1	100
232	ALM Br. 239	belt disc	type I-II	84.31	14.34	0.23	0.34	0.29	0.15	0	0.24	0.01	0.08	100
211	ALM LIIZ, 1g, 1	disc head pin	type l	83.56	14.85	0.26	0.34	0.53	0.11	0.01	0.19	0.03	0.1	100
195	ALM 94/1032, 4	neck collar, front	type I	83.33	15.79	0.16	0.21	0.29	0.05	0	0.05	0	0.12	100
212	ALM Br. 88	neck collar, inside	type I-II	83.19	15.67	0.19	0.33	0.33	0	0	0.1	0.02	0.16	100
196/197/265	ALM 3191	average neck collar	type II	81.68	16.45	0.54	0.35	0.63	0.14	0.03	60.0	0.017	0.13	100
234	ALM 7 (Br. 149, 17?)	neck collar fragment	type II	81.65	16.95	0.37	0.4	0.33	90.0	0.01	0.1	0	0.11	100

metal														
Q	museum-number	additional information	patina*	patina* Cu in %	Sn in %	Pb in %	As in %	Ni in %	Sb in %	Bi in %	Fe in %	% ui o	Zn in %	alloy in %
200	ALM Br. 438	neck collar	type I	81.13	16.84	0.2	0.28	0.14	0	0	1.27	0	0.13	100
217/218	ALM 4124	average neck collar	type I-II 79.72	79.72	17.71	0.37	99.0	0.98	0.125	0.04	0.19	0.03	0.16	100
227	ALM LIH16	belt disc	type II	76.4	21.27	0.11	0.77	0.64	0.33	0	0.34	0.03	0.12	100
249/250	ALM LIIQ, 3	average neck collar	type I-II	76.03	21.71	0.45	9.0	0.7	0.195	0.03	0.15	0.03	0.1	100
239/291/292	ALM LIIQ, 2	average neck collar	type II	76.02	23.3	0.04	0.09	0.05	0	0	0.39	0	0.09	100
236/237	ALM Br. 949	average neck collar	type I-II	76.02	22.71	0.04	0.08	0.09	0	0	0.91	0	0.14	100
226	ALM 26 (?)	neck collar, front	type I	74.86	21.96	1.19	0.5	0.52	0.17	60.0	0.55	0	0.15	100
219/220/256/257	ALM LIIQ 8	average neck collar	type I	72.95	25.35	0.56	0.34	0.27	90.0	0.03	0.24	0.01	0.18	100
221/259	ALM 2303	average neck collar	type I+	72.29	24.84	0.89	0.62	0.38	0.21	0,045	0.46	0.01	0.24	100
244/293	ALM LIIQ, 5	average neck collar	type I-II	67.33	29.31	1.67	0.55	0.36	0	0.07	0.46	0.01	0.23	100
210	ALM 2300	ring knive, ring	type I-II	66.82	30.34	0.75	0.72	0.59	0.16	0.04	0.29	0	0.3	100
229	ALM 2197	leg ring, inside	type II	66.37	30.29	1.87	0.48	0.27	0.18	0.03	0.38	0	0.13	100
222	ALM Br. 1204	neck collar	type I	66.02	30.63	0.03	0.43	0.4	0.79	0	1.54	0	0.15	100
201	ALM 2303	neck collar, coating	type I+	63.52	32.33	1.21	92.0	0.48	0.24	0.05	1.02	0.03	0.35	100
209	ALM 2300	ring knive, centre	type I-II	60.04	36.62	0.74	0.99	0.75	0.18	0.05	0.24	0	0.39	100
253	ALM 3374a	neck collar, less cor.	type I	52.98	33.63	0	0.44	0.25	0	0	12.47	0	0.23	100
242/243	ALM 2003/1201, 134	neck collar, coating	type I+	50.03	44.625	1.185	0.48	0.55	0.125	0.51	2.74	0.025	0.13	100
235/263/264	ALM 94/3/1	average neck collar	type I+	41.26	51.88	0.17	0.23	0	0	0.03	6.29	0	0.15	100
202/203/289/290	ALM LIIQ, 7	average neck collar	type II	41.13	56.4	0.97	0.34	0.09	0	0.04	0.88	0	0.13	100
288	ALM LIIQ, 7	neck collar piece	type III	32.7	63.33	1.85	0.51	0.17	0	0.1	1.22	0	0.13	100
208	ALM 2300	ring knive, tip	type I-II	32.5	32.78	31.79	0	0.23	0.84	0	0.18	0	1.68	100
213/214/255	ALM 3374a	average neck collar	type I	26.5	49.78	0.01	0.59	0.18	0	0	22.76	0	0.17	100

4 Conclusion and Perspective

Both non-destructive analysis by handheld XRF-devices and traditional XRF analysis of corroded bronze objects can provide useful but limited information about artefacts. In the first case, the results of these analyses can determine the morphology of corrosion crusts (see also results by Constantinides et al. 2002, Fernandes et al. 2013, Mircea et al. 2012, Wadsak et al. 2000). When considered alongside other factors (e.g. weight, colour (see for example Oudbashi et al. 2013, Weisser 1975, 207), and the characteristic changes of the surface by the various types of patina described above) can be used to inform the conservator about the state of an artefact.

Furthermore, such an analysis permits identification of the major elements present in the material used to craft the artefact. One can assess whether an artefact is made of copper, bronze, brass, silver, or gold. Thus, the non-destructive analysis using XRF will provide answers to most general questions regarding material. The same is also true for some copper alloys, like arsenic-bronze, tin-bronze and lead-bronze. Alloys high in lead are more resistant to corrosion due to a quick passive oxide layer of metallic lead (Fernandes et al. 2013, 5). It has also been illustrated that the significant dissolution of copper documented in other copper alloys does not occur in arsenic bronzes (Constantinides et al. 2002, 93). Thus, more detailed information regarding an artefact's original composition, which is also explored here, might be achieved.

However, this analysis has demonstrated that tin-bronzes are especially prone to both types of corrosion, and that major changes in composition are caused during the corrosion process. The type of corrosion, however, cannot be determined with any certainty by a visual, qualitative analysis. Additionally, several cases of bronze disease (type III) in which no metallic copper was left in the artefact could be identified in the material. Furthermore, by comparing SEM cross-section scans on artefacts contemporary to the pXRF-measured items from Mecklenburg, it became clear that the thickness of the corrosion crust differs greatly in several cases. Even after stripping off the corrosion elements, a mathematical extrapolation of the values could not yield any results comparable to the alloying ratios which are known from the Bronze Age.

Generally, a non-destructive, XRF-driven methodology is insufficient in identifying and quantifying the components of an artefact's alloy as intended by the craftsperson. This method cannot define intentionally improved alloys by specific craftspeople and, thus, is not suitable for the definition of workshops. Metallographic sampling, however, can help to identify craftspeople, as the skill of a craftsperson becomes apparent through the techniques that he/she applies. With regard to handheld XRF investigations of corroded bronze artefacts from museum collections, however, the fact remains that sampling is necessary in order to answer detailed questions related to provenance, workshops and craftspeople. That being said, XRF can nonetheless help to identify objects for further analysis, as heavily corroded objects are difficult to evaluate using metallographic methods.

Acknowledgements: The research leading to these results received funding from the European Union Seventh Framework Program (FP7/2007e2013) under grant agreement no. 212402. Additional special thanks go to the Archäologisches Landesmuseum Mecklenburg-Vorpommern and the Niedersächsisches Landesmuseum Hannover for their permission to investigate the artefacts and publish their images. My gratitude also goes out to the Mining Museum Bochum for providing the handheld XRF and SEM device, as well as the necessary knowledge and manpower to examine the corrosion depth of the artefacts. Special thanks to Rob Lee and Samantha Reiter for the English editing.

Supplementary Material

The online version of this article (DOI: 10.1515/opar-2017-0006) offers supplementary material.

Extended table 2: The data measured by the XRF device on the artefacts from Mecklenburg (German Mining Museum, Bochum) including elemental errors and full description of artefacts. In order to compare the measurements, the patina type is given based on a superficial examination (including visible profile sections) of the artefacts. Additional the corrosion elements are given in values.

References

- Anker, D. (1982). Die Röntgenfluoreszenzanalyse in der Archäologie. In K. d. R.-G. Zentralmuseums (Ed.), Festschrift Hans-Jürgen Hundt. Teil 3: Frühes Mittelalter (pp. 212-228). Mainz: Römisch-Germanischen Zentralmuseum Mainz.
- Bernard, M. C., & Joiret, S. (2009). Understanding corrosion of ancient metals for the conservation of cultural heritage. *Electrochimica Acta*, *54*, 5199-5205.
- Chase, W. (1994). Chinese bronzes: casting, finishing, patination and corrosion. In D. Scott, J. Podnay & B. Considine (Eds.), *Ancient and Historic Metals* (pp. 85-118). Cincinnati, Ohio: The Getty Conservation Institution.
- Constantinides, I., Adrianes, A., & Adams, F. (2002). Surface characterization of artificial corrosion layers on copper alloy reference materials. *Applied Surface Science*, 189, 90-101.
- Copper Development Association, I. (2008). Working with Copper. How to Apply Statuary and Patina Finsihes. https://www.copper.org/publications/pub_list/: Copper Alliance.
- Fernandes, R., van Os, B. J., & Huisman, H. D. (2013). The use of Hand-Held XRF for investigating the composition and corrosion of Roman copper-alloyed artefacts. *Heritage Science*, 1:30, 1-7.
- Groves, J. (2001, July of 2002). 16th Century Amber Varnish & Venetian Amber Varnish Amber Varnishes available during the 1500-1600's Retrieved 22-09, 2016.
- Harding, A. F. (2000). European Societies in the Bronze Age. Cambridge: Cambridge University Press.
- Helfert, M., & Böhme, D. (2010). Herkunftsbestimmung von Römischer Keramik mittels portabler energiedispersiver Röntgenfluoreszenzanalyse (P-ED-RFA) - erste Ergebnisse einer anwendungsbezogenen Teststudie. In B. Ramminger & O. Stilborg (Eds.), Naturwissenschaftliche Analysen vor- und frühgeschichtlicher Keramik I. Methoden, Anwndungsbereiche, Auswertungsmöglichkeiten (Vol. 176, pp. 11-30). Bonn: Dr. Rodolf Habelt GmbH.
- Härke, H. (1978). Probleme der optischen Emissionsspektralanalyse: Technische Möglichkeiten und methodische Fragestellungen. *Prähistorische Zeitschrift*, 53, 165-276.
- Junghans, S., Sangmeister, E., & Schröder, M. (1974). *Kupfer und Bronze in der frühen Metallzeit Europas*. Berlin: Mann. Laux, F. (1971). *Die Bronzezeit in der Lüneburger Heide*. Hildesheim: August Lax Verlag.
- Lutz, J., & Pernicka, E. (1996). Energy Dispersive X-Ray Fluorescence analysis of ancient Copper Alloys: Empirical Values for Precision and Accuracy. *Archaeometry*, 38, 2, 313-323.
- Mircea, O., Sandu, I., Vasilache, V., & Sandu, I. G. (2012). A study on the Deterioration and Degradation of Metallic Archaeological Artifacts. *International Journal of Conservation Science*, 3(3), 179-188.
- Nørgaard, H. W. (2011). Die Halskragen der Bronzezeit im nördlichen Mitteleuropa und Südskandinavien (Vol. 200). Bonn: Dr. Rudolf Habelt.
- Nørgaard, H. W. (2014a). Craftsmanship and Metalwork in the Nordic Bronze Age: craft organisation, craftspeople and their areas of contact. (PhD), Aarhus University, unpublished PhD-thesis.
- Nørgaard, H. W. (2014b). Valued Craftsmen: As important as prestige goods? -Some ideas about itinerant craftsmanship in the Nordic Bronze Age. In S. Reiter, H. W. Nørgaard, Z. Kolzce & C. Rassmann (Eds.), Rooted in Movement. Aspects of Mobility in Bronze Age Europe (pp. 37-52). Aarhus: Jutland Archaeological Society.
- Nørgaard, H. W. (2015a). Genau hingesehen Metallhandwerk in Mecklenburg zwischen 1550-1100 BC. Herstellungsspuren und Metallkompositionen als Indikator für Metallwerkstätten in Mecklenburg. *Bodendenkmalpflege in Mecklenburg-Vorpommern, Jahrbuch 61, 2013* (pp. 57-100). Schwerin: Abteilung Landesarchäologie im Landesamt für Kultur und Denkmalpflege Mecklenburg-Vorpommern.
- Nørgaard, H. W. (2015b). Metalcraft within the Nordic Bronze Age: Combined metallographic and superficial imaging reveals the technical repertoire in crafting bronze ornaments. *Journal for Archaeological Science*, 64, 110-128.
- Nørgaard, H. W. (2015c). Tracing the Hand that Crafted: how individual working traces make Bronze Age ornaments talk. In P. Suchowska-Ducke, S. S. Reiter & H. Vandkilde (Eds.), Forging Identities. The Mobility of Culture in Bronze Age Europe. Report from a Marie Curie project 2009-2012 with concluding conference at Aarhus University, Moesgaard 2012. (pp. 101-110). Oxford: BAR International Series.
- Otto, H. (1973). Über die Auswertung der Metallanalysen in Band 1 und 2 der "Studien zu den Anfängen der Metallurgie" (SAM). Acta Praehistoria et Archaeologica, 4, 1-9.
- Oudbashi, O., Emami, S. M., Ahmadi, H., & Davami, P. (2013). Micro-stratigraphical investigation on corrosion layers in ancient Bronze artefacts by scanning electron microscopy energy dispersive spectrometry and optical microscopy. *Heritage Science*, 1:21, 1-10.
- Pernicka, E. (1995). Gewinnung und Verbreitung der Metalle in prähistorischer Zeit. *Jahrbuch des Römisch-Germanischen Zentralmuseums Mainz*, *37. Jahrqanq*(Teil 1), 21-129.
- Pernicka, E. (2010). Archäometallurgische Untersuchungen am und zum Hortfund von Nebra. In H. Meller & F. Bertemes (Eds.), Der Griff nach den Sternen. Intern. Symposium Halle (Saale) 16.-21. Februar 2005 (pp. 719-734). Halle: Landesmuseums für Vorgeschichte.
- Pernicka, E. (2014). Provenance Determination of Archaeological Metal Objects. In B. W. Roberts & C. P. Thornton (Eds.), *Archaeometallurgy in Global Perspective. Methods and Syntheses* (pp. 239-268). London: Springer.

- Robbiola, L., Blengino, J.-M., & Fiaud, C. (1998). Morphology and Mechanisms of formation of Natural Patinas on Archaeological Cu-Sn Alloys. *Corrosion Science*, 40(12), 2083-2111.
- Sangmeister, E. (1971). Aufkommen der Arsenbronze in SO-Europa. In G. Novak (Ed.), Actes du VIIe Congres International des Sciences Prehistoriques et Protohistoriques, Beograd, 9-15 Septembre 1971 (pp. 109-129). Beograd.
- Šatović, D., Desnica, V., & Fazinić, S. (2013). Use of portable X-ray flourescence instrument for bulk alloy analysis on low corroded indoor bronzes. *Spectrochimica Acta Part B, 89*, 7-13.
- Stos-Gale, Z. A., & Gale, N. H. (2009). Metal provenancing using isotopes and the Oxford archaeological lead isotope database (OXALID). *Archaeological and Anthropological Sciences*, 1(3), 195-213.
- Wadsak, M., Constantinides, I., Vittiglio, G., Adriaens, A., Janssens, K., Schreiner, M., Wuttmann, M. (2000). Multianalytical Study of Patina Formed on Archaeological Metal Objects from Bliesbruck-Reinheim. *Mikrochimica Acta, 133*, 159-164.
- Weisser, T. S. (1975). The de-alloying of copper alloys. In N. S. Brommelle, P. Smith, D. Leigh, A. Moncrieff, W. A. Oddy & P. Pratt (Eds.), *Conservation in Archaeology and the Applied Arts*. (pp. 207-214). London: The international Institute for Conservation of Historic and Artistic Works.
- Wolff, T. (2009). Referenzprobenfreie quantitative Mikri-Röntgenfluoreszenzanalyse. Berlin.
- Wolters, J. (1991). Der Gold- und Silberschmied. Werkstoffe und Materialien. Stuttgart.